Mn^{4+}-activated oxyfluoride K_3TaOF_6 red phosphor with intense zero phonon line for warm white light-emitting diodes

Jiao Wu[a], Bo Wang[a]*, Zhiyuan Liu[a], Kang Zhang[a] and Qingguang Zeng[a]*

[a]School of Applied Physics and Materials, Wuyi University, Jiangmen, Guangdong 529020, P.R. China

Corresponding Authors: wangbo312@mails.ucas.ac.cn; zengqg@mail.ustc.edu.cn

Characterizations

The phase composition of $K_3TaOF_6:Mn^{4+}$ were measured by a powder diffractometer (X' Pert PRO, Cu Kα, λ = 1.5418 Å). The photoluminescence (PL) spectra were recorded by Edinburgh Instruments (FLS 980) equipped with 450 W xenon lamps as the excitation source. The diffuse refection spectra (DRS) of the samples were carried out on an UV-Vis-NIR spectrophotometer (Lambda 950, Perkin Elmer), using $BaSO_4$ as a standard reference. The morphologies of the samples were characterized using a scanning electron microscope (SEM, JSM-6700F). A LTTL-3DS measurement was used to record the 3D TL glow curves at a heating rate of 1 K/s. Each sample was firstly irradiated under Hg UV light for 3 min, and then kept in the dark for 5 min. The electron paramagnetic resonance (EPR) spectrum of $K_3TaOF_6:Mn^{4+}$ was obtained on a JES-FA 200 EPR spectrometer. High-resolution transmission electron microscopy (HRTEM) was recorded using a FEI Tecnai G2S-Twin.

Figure Caption

Fig. S1. (a-c)The Rietveld analysis for K_3TaOF_6:xMn^{4+} sample on the XRD data (d) Cell volumes as a function of composition x.

Fig. S2. (a) Room temperature DRS of K_3TaOF_6:xMn^{4+} (b) host bandgap calculated from the reflectance spectrum.

Fig. S3. (a) The concentration-dependent integrated emission intensity. (b) the decay curves of K_3TaOF_6:xMn^{4+} samples.

Fig. S4. (a) Tanabe-Sugano energy diagram for Mn^{4+} ($3d^3$) in an octahedral crystal field (b) The relationship between the Mn^{4+}:^2E energy level and the calculated nephelauxetic ratio in different β hosts.

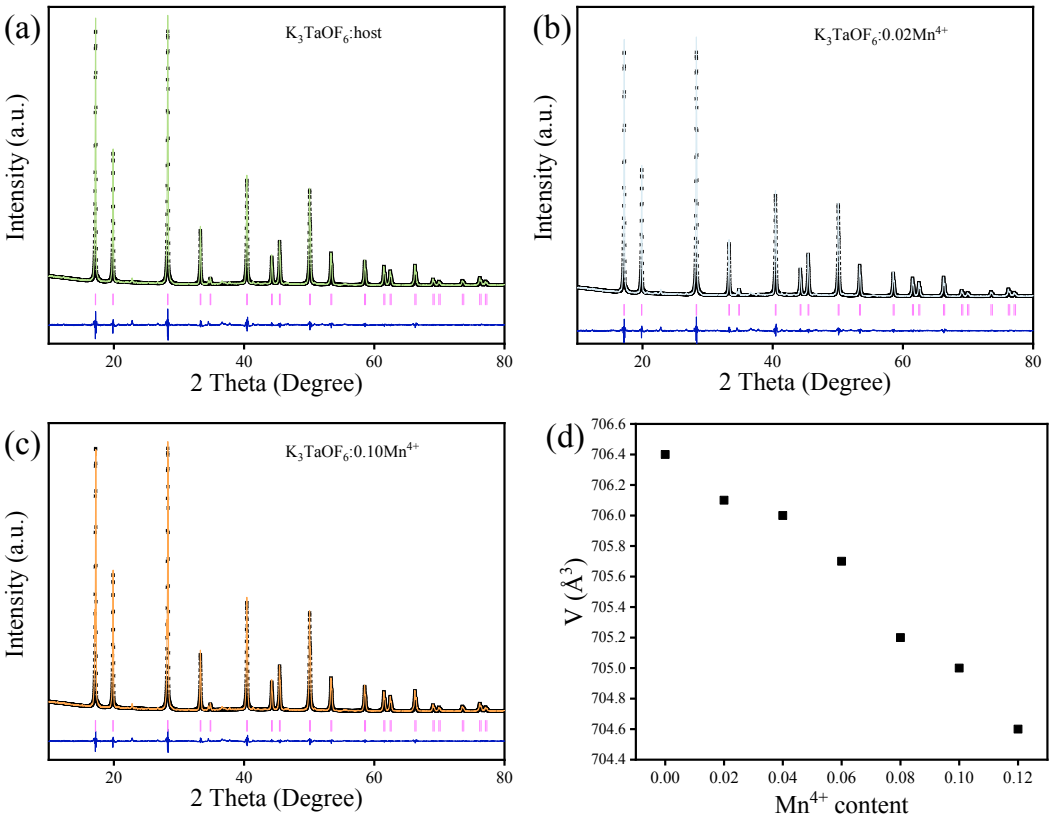

Fig.S1. (a-c)The Rietveld analysis for K_3TaOF_6:xMn^{4+} sample on the XRD data (d) Cell volumes as a function of composition x.

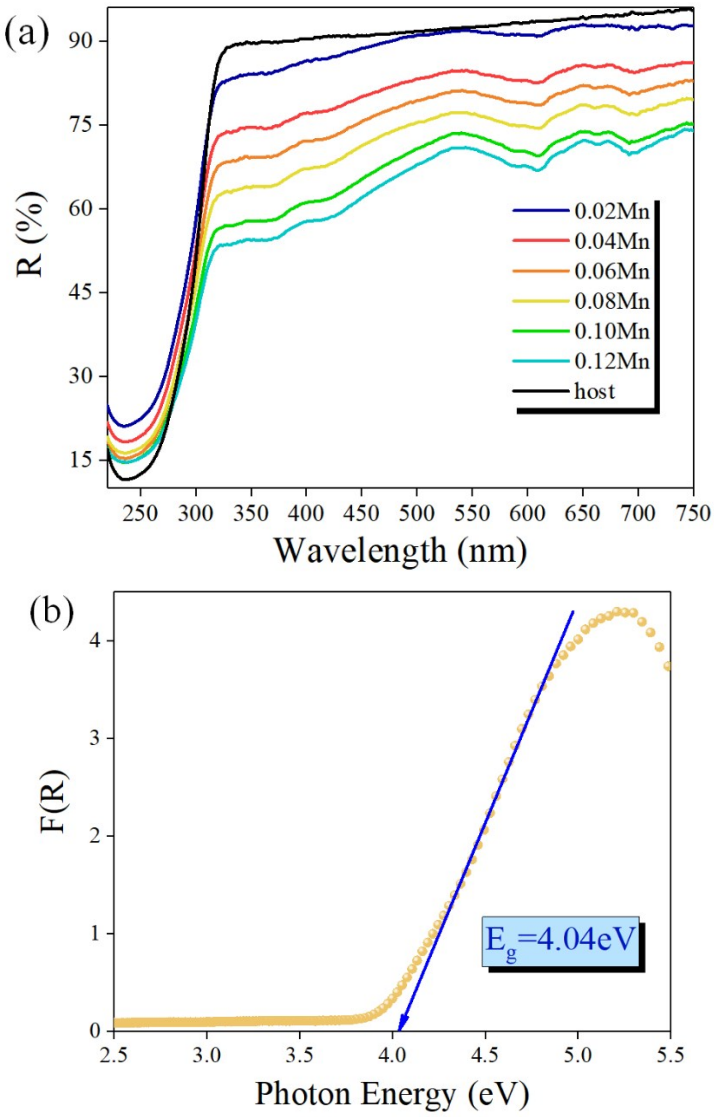

Fig. S2. (a) Room temperature DRS of K_3TaOF_6:xMn^{4+} (b) host bandgap calculated from the reflectance spectrum.

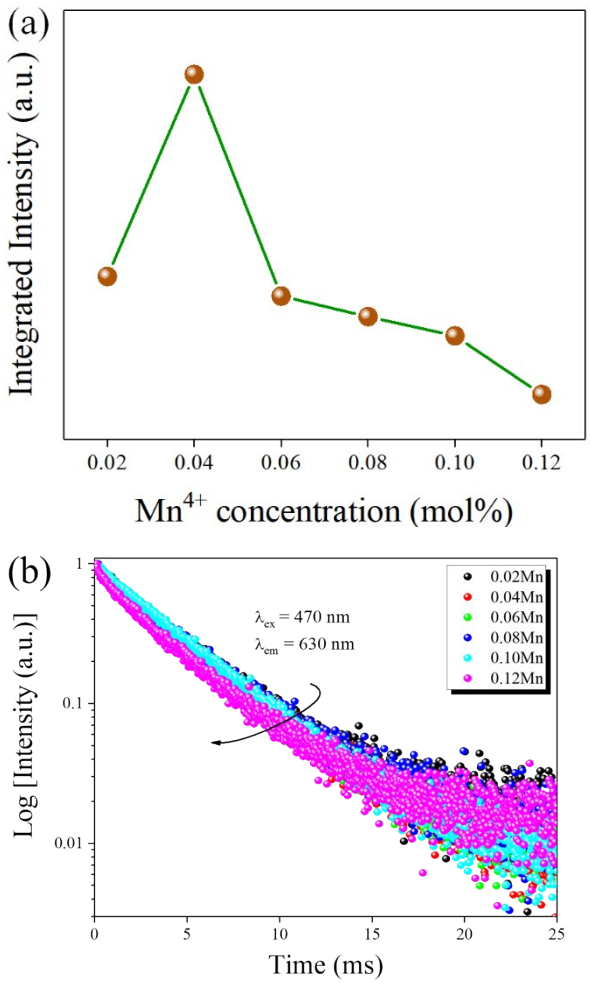

Fig. S3. (a) The concentration-dependent integrated emission intensity. (b) the decay curves of K_3TaOF_6:xMn^{4+} samples.

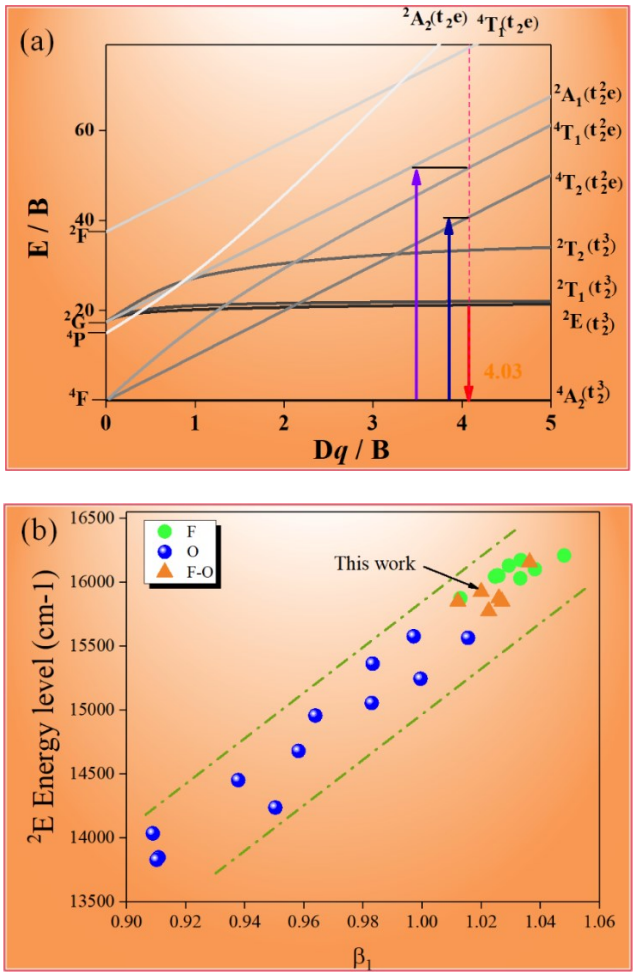

Fig. S4. (a) Tanabe-Sugano energy diagram for Mn^{4+} ($3d^3$) in an octahedral crystal field (b) The relationship between the Mn^{4+}:^2E energy level and the calculated nephelauxetic ratio in different β hosts.